INSTITUTE OF PHYSICS PUBLISHING JOURNAL OF PHYSICS: CONDENSED MATTER

J. Phys.: Condens. Matter **14** (2002) 5325–5336 PII: S0953-8984(02)33883-9

Ab initio study of tetragonal variants in Ni_2MnGa alloy

A Ayuela, J Enkovaara and R M Nieminen

Laboratory of Physics, Helsinki University of Technology, 02015 Espoo, Finland

Received 2 April 2002
Published 16 May 2002
Online at stacks.iop.org/JPhysCM/14/5325

Abstract

A major challenge for the study of the magnetically shape-controlled memory alloys Ni–Mn–Ga is the structural search for their variants. We report studies of the variants of Ni_2MnGa alloys from a theoretical point of view by means of density functional calculations using the generalized gradient approximation. The effect of tetragonal distortions is studied, and a metastable structure is found for $c/a = 0.94$, in agreement with experiments. The $c/a < 1$ minimum is reinforced by considering volume expansions around the experimental values for several variants. After distortion, the electron density is redistributed around the Ni atoms as shown by neutron scattering experiments. The previous disagreement between the theoretical spin density and the experimental neutron scattering is explained. In addition, elastic constants and x-ray absorption spectra are calculated in order to encourage measurements of these quantities.

(Some figures in this article are in colour only in the electronic version)

1. Introduction

There are many useful applications for the shape memory effect (SME), the basis of which lies in the martensitic transformation of metallic alloys. While the SME is conventionally driven by temperature, a faster control could be reached by using an external magnetic field. Such is the case for the ferromagnetic Ni–Mn–Ga alloys around the stoichiometric Ni_2MnGa, the structure and electronic properties of which are the topic of this paper.

The martensitic transformation is based on a structural deformation from a high-symmetry structure to lower symmetry. For practical applications, the lower-symmetry structures should be stable at room temperature, i.e. the temperature of the martensitic transformation T_M should be higher than room temperature. For Ni–Mn–Ga ferromagnetic materials, the martensitic transformation has its origin in a tetragonal distortion of the ordered structure $L2_1$, which is shown in figure 1. The $L2_1$ structure has the lattice parameter $a = 5.826$ Å [2], while other structures, called variants, show the following order when lowering temperature:

(i) a tetragonal structure with a ratio $c/a < 1$,
(ii) an arrangement close to an orthorhombic structure [3, 4] and
(iii) another tetragonal structure with $c/a > 1$.

0953-8984/02/215325+12$30.00

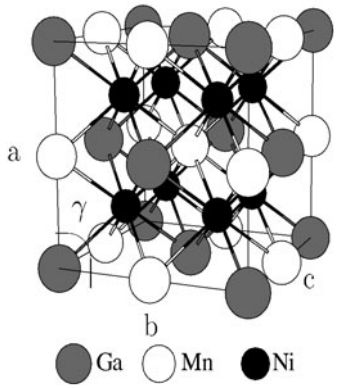

Figure 1. Unit cell of Ni_2MnGa in the cubic $L2_1$ structure.

In cases (i) and (ii) the low-symmetry structures can exhibit shuffling of the [110] planes with a modulation of five and seven atomic planes, called 5M and 7M structures in the literature, respectively [5–7]. In general, the characterization of the structures below the martensite temperature depends strongly on the alloying composition, which implies changes in the electronic concentration. Furthermore, additional structural information around the equilibrium positions is given by the elastic constants as determined by ultrasound experiments [8, 9]. Specifically, thin-film processing exploits the softness of the martensitic distortions in order to grow epitaxially ferromagnetic Ni_2MnGa on different substrates, for instance on GaAs(001) using a NiGa interlayer [10] or a ScErAs [11] interlayer.

New experiments concerning these structural and thermal aspects have aroused interest in these compounds [12]. For the magnetic control aspects, large strains ($\sim$5%) for single crystals, close to the maximum tetragonal distortion, are measured under magnetic fields around 0.5 T [13, 14]. These strain values clearly exceed the typical values ($\sim$0.1–0.24%) which characterize both magnetostrictive and piezoelectric materials.

A better magnetic control is obtained when a smaller field can be applied, i.e. it calls for ferromagnetic materials with a large magnetic moment. Previously measured magnetic properties give $\mu = 4.17\ \mu_B$ per formula unit for the perfect $L2_1$ structure [2]. A more detailed magnetic analysis per element has also been performed [1] by means of polarized neutron scattering measurements. In [1] the authors also look for the electronic origin of the effect of the tetragonal distortions as due to the splitting of a peak in the density of states (DOS) close to the Fermi level. This new experiment concentrates on our previous results [15], which in addition concentrate the search for new ferromagnetic candidates by looking for the element dependence of the distortions, as the electronic concentration varies with changing the elements. In [15], we study computationally the perfect stoichiometric compound Ni_2MnGa, where, however, the tetragonal variant with $c/a < 1$ was not clearly seen. In the meantime, several papers have appeared with various micromagnetic models at the mesoscopic level [16, 17], also including a thermodynamic model for the free energy at the macroscopic level [18]. It has also been shown that an atomic simulation can be based on pseudopotential calculations [19] for these ternary Ni–Mn–Ga compounds. All this new experimental and theoretical evidence shows some limitations in our previous study and indicates that a more comprehensive study of the Ni_2MnGa alloy is needed. Here, we concentrate on the Ni–Mn–Ga compounds and search for the origin of tetragonal distortions with different volumes.

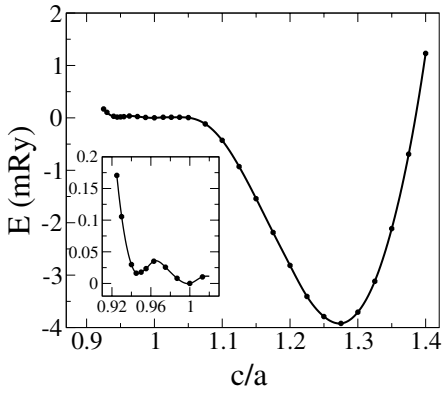

Figure 2. Total energy difference $\Delta E_{tot}^{distorted}$ (relative to the $L2_1$ phase and per formula unit) as a function of c/a in the tetragonal distortions for the equilibrium theoretical volume.

As a first step, as in our previous study, we perform *ab initio* full-potential-linear-augmented-plane-wave (FLAPW) calculations, for which the computational details are briefly described in section 2. Our assumption for this work is that, although the calculations are made at zero temperature, the different structures below the martensite temperature should appear at least as metastable minima. In a second step, as described in section 3, we investigate the role of the volume on the distortions. Other electronic and structural properties, in particular the elastic constants and x-ray absorption spectra (XANES), are calculated. Other interesting aspects, which are left for further work, include, for example, the match between low-symmetry variants to form twins and the swapping of twins through the sample with a certain time dependence.

2. Computational details

The calculations have been performed within the density-functional theory using the FLAPW method as implemented in the WIEN code [20]. The FLAPW method is among the most accurate band structure methods currently available. The exchange–correlation potential is approximated by the generalized-gradient approximation (GGA) of Perdew *et al* [21]. The maximum l value in the radial sphere expansion is $l_{max} = 10$, and the largest l value for the non-spherical part of the Hamiltonian matrix is $l_{max,ns} = 4$. The cut-off parameters are $RK_{max} = 9$ for the plane waves and $G_{max} = 14$ for the charge density, so that no shape approximation to the potential occurs.

3. Results

3.1. Tetragonal distortions

In this section we analyse in more detail the tetragonal distortions. As in our previous work [15], the seed $L2_1$ structure (figure 1) for the distortions is obtained with an equilibrium lattice constant of 5.81 Å, where the number of non-equivalent atoms is four. The Brillouin zone integrations are carried out with an accurate scheme by using special points generated with the improved tetrahedron method: the number of k-points is ≈8000, i.e. 641 in the irreducible Brillouin zone. In order to deal with the core electrons and the local orbitals in different computational schemes, the muffin-tin radii are choosen to have the following values: Ga 1.19 Å, Mn 1.27 Å and Ni 1.19 Å. The interstitial region gives a very small magnetic contribution.

Table 1. Local magnetic moments per site in units of μ_B. Experimental values (Exp.) are obtained from [1].

		Ni	Mn	Ga
$L2_1$ cubic	Th.	0.36	3.43	−0.04
	Exp.	0.24	2.74	−0.013
$c/a = 0.94$	Th.	0.4	3.43	−0.04
	Exp.	0.36	2.83	−0.06

In figure 2, the energy as a function of the tetragonal c/a ratio appears mostly as before [15], but as we do not use any smearing in this case the region around $c/a = 1$ becomes better resolved. Further details of the tests performed in this case are given in the appendix. The inset of figure 2, with a higher resolution, shows a minimum for $c/a < 1$ with a small energy barrier, about 0.34 meV. The energy scale in order to pinpoint the $c/a < 1$ minimum is smaller when compared with the variant with $c/a > 1$. The small energy difference explains the missing of the $c/a < 1$ minimum in previous calculations. Moreover, the energy to pass the barriers involved in the distortion process is related to the latent heat. The experimental estimate of the latent heat for this kind of alloy ranges in the interval 0.9–5.0 meV/formula unit [22]. The theoretical barriers and experimental latent heats are comparable in this case, and we can reproduce the experimental variants. One can say that the variant with $c/a > 1$, with smaller energy, will appear at low temperatures. This finding has been recently confirmed by means of x-ray diffraction experiments [23]. Although the temperature dependence of the variants deserves further work, which is beyond the scope of this paper, a more detailed study of the volume dependence of the minima at $c/a < 1$ and $c/a = 1$ is also needed. This question is further analysed in section 3.1.1 below.

Here, we claim only the appearance of the $c/a = 0.94$ minimum, which corresponds to one kind of martensite. The stabilization of the $c/a > 1$ phase can be performed when including the role of the temperature via vibrational entropy [24]. On the other hand, as the minima $c/a = 1$ and <1 stay in a flat area and the energy barriers are small, we think that the stabilization of the $c/a < 1$ phase against the $c/a = 1$ one would require dealing with the role of the magnetism via the entropy terms. However, this subject is beyond the scope of our present paper.

Concerning electronic aspects, we obtain the magnetic moment as a function of the distortion, shown in figure 3. The magnetic moments per site are given in table 1. The magnetic moments of the interstitial region do not change the results appreciably. Experimentally, the total magnetic moment is 4.17 μ_B for the $L2_1$ cubic structure [2], and the magnetic moments per site obtained from the polarized neutron scattering and after extrapolating to zero temperature [1] are also presented in table 1. Our theoretical results agree with the experiment in giving a higher total moment due to transition metals in the tetragonal phase. In addition the Ni moment follows the total magnetic variation around $c/a = 1$ because two Ni atoms contribute to the total magnetic moment, so the uniform change of Mn atoms is masked. These findings suggest that the Ni contribution to the total changes in magnetic moments is larger with respect to Mn, with a small redistribution of moments which is in complete agreement with experiments. This agreement contradicts the comparison with earlier calculations [25] where the total transition-element moment decreases when going to the tetragonal phase. In addition, the moment redistribution in [25] should take into account the Mn atom. The performance of our calculations with a full potential and with a better correlation scheme seems to be critical for the detailed description of these alloys, as has been emphasized already in the context of volume relaxations [15].

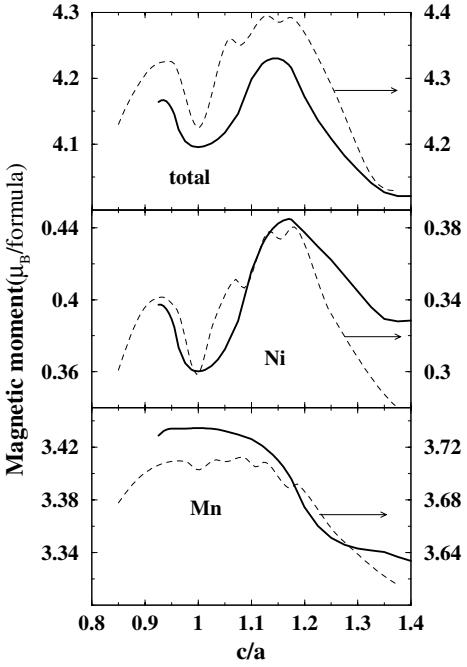

Figure 3. Total magnetic moment and contributions associated with individual atoms in Ni_2MnGa as a function of the c/a ratio. Broken curves give the values from [19].

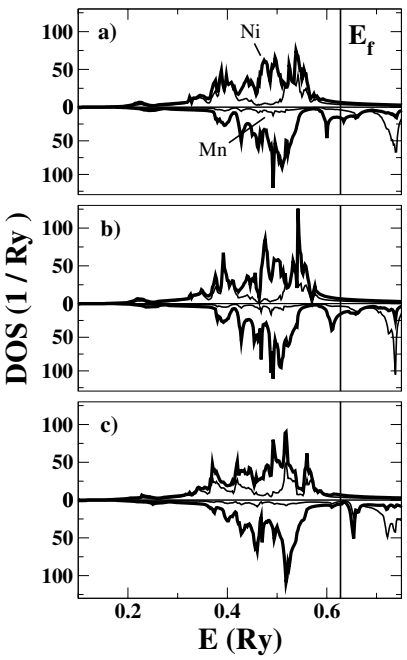

Figure 4. Site spin-projected d-electron state densities for Ni (thick curve) and Mn (thin curve) for the minima of figure 2: $c/a < 1$ (a), $c/a = 1$ (b) and $c/a > 1$ (c).

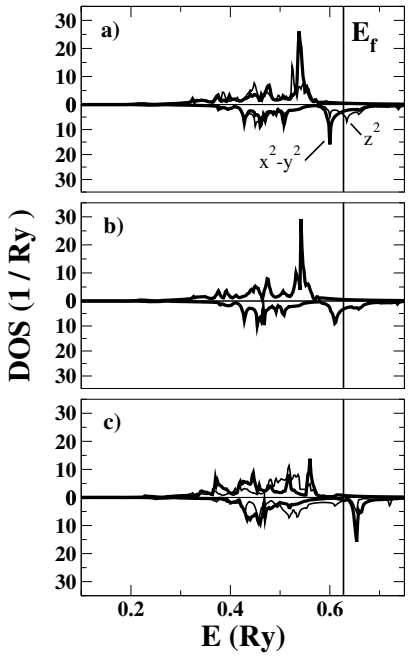

Figure 5. Decomposed Ni spin-projected d-electron state densities as in the previous figure.

Let us next look deeper into the electronic origin of the distortions. The variation of the magnetic moment in the Ni site is associated with a variation of the local density of states (LDOS) due to Ni, as seen in figure 4. The Fermi level lies just above a peak in the LDOS of the minority-spin Ni e_g band, and the level lies for the Mn band in a position at which there is almost an equal LDOS of majority and minority t_{2g} states. This is in agreement with the experiments of [1]. Contrary to [1], the partial LDOS in figure 5 offers a different interpretation, which is detailed in the following.

(i) For $c/a < 1$, the peak in the minority Ni e_g band is split and narrowed with respect to the cubic structure during the tetragonal transition, whereas there is little change in the Mn bands near the Fermi surface. The e_g band has a $d_{x^2-y^2}$ character, while the d_{z^2} band lies mainly above the Fermi level. The latter band is broader than the former due to the proximity of Ni–Ga atoms, which brings into play a larger hybridization of Ni atoms with the p-states of Ga atoms [26].

(ii) When the ratio $c/a > 1$, the $d_{x^2-y^2}$ and d_{z^2} bands of mainly Ni character reverse their order. Also the band broadening increases because the equilibrium deformation for $c/a > 1$ is larger than for $c/a < 1$. In fact, related to this larger broadening, the Mn peaks for this kind of deformation $c/a > 1$ vary to a larger extent than with $c/a < 1$. This is logical because the atoms in the $c/a < 1$ case hybridize more as they become closer to each other within the a–b plane for $c/a > 1$.

The change of the electronic density on the different distortions for the $c/a < 1$ minimum is shown in figure 6, which gives the reconstruction of the magnetization distribution in a section through the origin parallel to the $[1\bar{1}0]$ plane. There is a negative spin density difference at the Mn site and a non-negligible positive density difference at the Ni site, so that the magnetization is redistributed differently in the Mn than in the Ni during the tetragonal transition. The negative

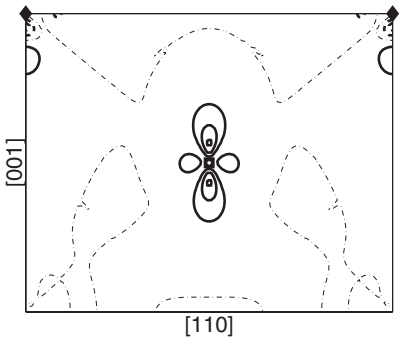

Figure 6. Redistribution of magnetization which occurs due to the transformation from the cubic structure to the tetragonal structure with $c/a < 1$. The plot shows the section parallel to [110] passing through the origin. The contour intervals are at 0.125 μ_B Å^{-3}; negative contours are shown as dashed curves. The dot–dashed curves show the zero-contour level.

density difference is extended along the [110] direction, and it is consistent with the depletion of the d_{xy} orbitals around Mn. The positive density difference at the Ni site is elongated along the z axis and is consistent with the decrease in the number of unpaired electrons for the d_{z^2} orbital. Our findings are fully in agreement with the experiments [1]. However, the order between z^2 and $x^2 - y^2$ given in the interpretation of [1] must be reversed, and the discussion based on the capture of electrons by the d_{z^2} orbital along the deformation should be reconsidered.

Our results can also be compared with the pseudopotential results of [19]. The authors used a local-spin-density (LSD) scheme for the treatment of the electronic correlation, together with pseudopotentials. When looking at the energy versus c/a deformations, the region with $c/a > 1$ in the pseudopotential calculations shows additional minima. These minima are also correlated with magnetic moment maxima, which are spurious according to our results. Specifically, our Mn local magnetic moments show no oscillation in the $c/a > 1$ range. The change in magnetic moment in our case is mainly due to Ni, as seen in figure 3. Godlevsky and Rabe [19] do not observe the minimum with $c/a < 1$, which is very tiny even in our model. This can be understood because the peak in the minority DOS below the Fermi level shows a smaller splitting for the pseudopotential case.

3.1.1. Volume. Next we investigate how the case for the $c/a < 1$ minimum can be reinforced. As previously commented, the mechanism for the appearance of this minimum relies strongly on the peak around the Fermi level. Whenever the Ni DOS minority peak moves closer to the Fermi level, the situation favours the splitting of this peak through distortions. One possibility is to make the Ni band narrower, for instance by increasing the volume. In a more detailed manner, we can infer the changes in the DOS when increasing the volume. In such a case, the peak around the Fermi level already moves closer to the Fermi level in the cubic phase. By adding the distortions, the splitting of this peak decreases the energy for both sides of the distortions, $c/a \lesseqgtr 1$, i.e. it favours the desired trends. Naturally, both distortion ratios will approach the cubic structure as they become more symmetric. Everything guides us to think that the tetragonal distortion with $c/a < 1$ could be further stabilized by a change in volume, which for instance could be driven by a departure from the stoichiometric composition. As an illustration, we investigate here the tetragonal distortions when varying the unit-cell volume.

Here, we use the previous parameters for the calculations [15]: The muffin-tin sphere radii R_{MT} are 1.11 Å for Ni, 1.16 for Mn and 1.27 for Ga. The number of special $\boldsymbol{k}$-points

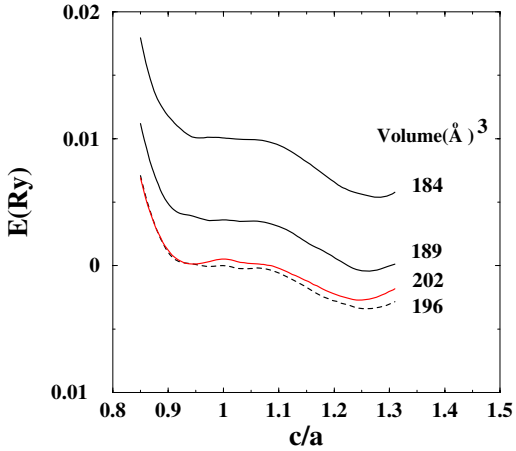

Figure 7. As in figure 2 for different volumes. The zero of energy refers to the equilibrium $L2_1$ volume with $c/a = 1$.

Table 2. Elastic constants in units of GPa. For the experimental values see the text.

	Theory	Experiments
$L2_1$	4	4.5, 22
$c/a = 0.94$	12	7.6
$c/a = 1.26$	30	

decreases in the irreducible Brillouin zone integration to 172 for a bct substructure from figure 1. The tetragonal deformations for several volumes around the experimental values are given in figure 7.

The equilibrium volume curve, 196 Å^3, has two minima at $c/a = 0.94$ and 1.26, weak as we commented in the previous section. For smaller volumes the inner minimum with the $c/a < 1$ disappears, while the energy of the position with $c/a > 1$ is lower with respect to the cubic structure, $c/a = 1$. For larger volumes the most important result is that the $c/a < 1$ minimum is reinforced. Also, as the volume increases, the minimum around $c/a = 1.25$ rises relative to the cubic structure. However, these trends for varying volumes are opposite to the pseudopotential calculations of Godlevsky and Rabe [19]. Our results confirm the splitting of the peaks as we discussed at the beginning of this section. It appears that the martensitic transformation should disappear under a hydrostatic pressure, giving rise to a homogeneous volume change.

A last question is the change in the equilibrium volume for the other minimum, $c/a \gtrless 1$, in figure 2. We have checked the case corresponding to the larger distortion in the minimum $c/a > 1$. The volume change with respect to the $L2_1$ phase is 0.2 Å^3 and the change in energy is two orders of magnitude lower than the calculated barrier between the $L2_1$ and the $c/a < 1$ phase. It seems that the change of volume between the respective minima is negligible.

3.1.2. Elastic shear constants. As seen in figure 2, the total energy corresponding to these tetragonal distortions for this compound exhibits several minima for which the elastic shear constant C' can be calculated. They are computed by means of second derivatives of the energy density as $U = 6C'\delta^2$ at the required minima. As these elastic constants are small,

their estimated values C' are around 4 and 12 GPa for the $L2_1$ structure and the tetragonal structure with $c/a < 1$ respectively, and 30 GPa for $c/a = 1.26$, as compiled in table 2. They compare well with the experimental values for the $L2_1$ structure obtained by ultrasonic measurements, which give values for C' between 4.5 [8] and 22 GPa [9]. Also the elastic constant C' for a variant $c/a < 1$ agrees with the measured value of 7.6 GPa, by means of Young constant elastic measurements close to the martensite temperature [27].

The discrepancy in the experimental values seems to be due to differences in the crystal stoichiometry. For instance, in the experimental alloy of [27] Ga is replaced by Mn while the Ni composition remains approximately the same. As this replacement decreases the volume with respect to the ideal stoichiometry, C' for $c/a < 1$ becomes lower as seen in figure 7. The lowering can bring into even better agreement the theoretical and experimental values. However further work will be needed to address this issue quantitatively.

On the other hand, the ratio C_{44}/C' may be used as an anisotropy factor for cubic crystals ($C_{44}/C' = 1$ for an elastically isotropic material). Here the crystal stoichiometry affects mainly C' as suggested by the experiments [8, 9]. For the example discussed in the previous paragraph, we obtain a higher anisotropy effect because the elastic shear will decrease. The calculations are reported here in order to encourage experimentalists to measure the elastic constants in the martensitic phase, as they are considered key parameters for the distortions of the variants.

3.2. XAS

The density of Mn d and/or Ni d hybridized states around the Fermi level in the Ni_2MnGa system should be observable for all excitations involving outermost Mn d or Ni d final states from x-ray-absorption-near-edge-structure (XANES) spectra. The chemical shifts of the adsorption edge in the XANES spectra are strongly related to the charge transfer between the different sites. Here we analyse the electronic structure of Ni_2MnGa by combining studies on the Ni and Mn $L_{3,2}$ lines. The Mn and Ni x-ray emission spectra (XES) of the $2p_{3/2}$ electrons have been measured [28]. In addition, there are results for the x-ray photoelectron spectra (XPS) which reflect a distribution of d electrons in the valence zone.

For the analysis, one needs to know more about the separation and the relative intensity between the lines L_α and L_β, i.e. the spectrometer resolution and the peak lifetimes. The spin–orbit splitting is taken as 10.4 eV, and it can be identified as the distance between the two centres of energy of the $p_{3/2}$ and $p_{1/2}$ states, in agreement with x-ray emission observations from other Heusler alloys containing Ni and Mn [29]. The ratio L_β/L_α is also chosen as 0.7 from these experiments. Simultaneously a final lifetime for the core hole has been simulated by introducing a lifetime broadening of 0.4 eV. Naturally the main peak of Mn could be split due a Zeeman-like effect because the Mn atom is carrying most of the magnetic moment. However, in our calculations, we have not considered this splitting. These results are calculated using the code developed by Ambrosch-Draxl *et al* [30] as implemented in our FLAPW code [20].

The absorption spectra for the $L2_1$ structure and the tetragonal structure $c/a = 0.94$ are given in figure 8. The spectra given by full curves for all three atoms are also decomposed into spin-up and spin-down parts, as shown by the broken curves. As a general feature, the Mn main peak is located at higher energies than the Ni main structure. This is in agreement with the emission measurements, although it is important to note that no information about the quality of the sample is available. There is a need to complement these experiments with absorption measurements in order to compare directly with our calculations [28]. Equally important, the arrows refer to the main differences between the structures. They differ around the binding energy of 5 eV for all the elements. In contrast, the first peaks only show a difference for Ni.

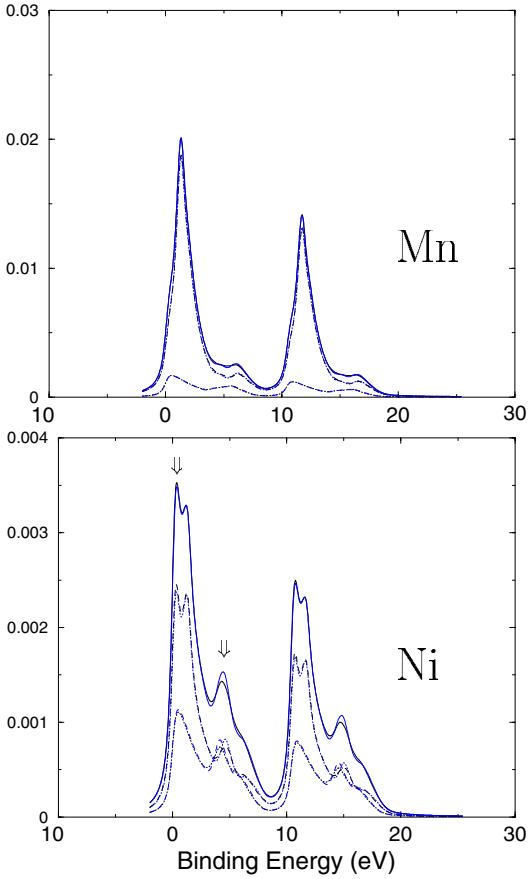

Figure 8. $L_{3,2}$-edge XANES for Mn (a) and Ni (b) for $c/a = 1$ (blue) and $c/a = 0.94$ structures (black). The decomposition into up and down parts is given by dashed curves: larger values represent spin up while lower values are spin down.

It appears that extra measurements should be carried out because the differences seem large enough to be experimentally discriminated.

4. Conclusions

We have studied in detail Ni–Mn–Ga alloys, in particular the tetragonal structures with $c/a < 1$. We assume that density-functional calculations are able to describe the topology of the energy versus distortion. When one neglects the role of temperature, three minima should be present. We reproduce the experimental minimum with $c/a < 1$. This result can be explained by electronic aspects of the distortion: the DOS splitting around the Fermi level is mainly due to Ni, and the character of the involved bands is $d_{x^2-y^2}$ and d_{z^2} for the $c/a < 1$ variant and for the $c/a > 1$ variant, respectively. The effective value of the splitting is proportional to the deformation. These findings explicitly corroborate the DOS analysis for other compounds [15]. In line with these results the electronic density is also examined and shows agreement with the neutron scattering experiments. These results provide evidence that the neutron scattering experiments must be reinterpreted, and the failed agreement between the experiment and the previous calculations disappears.

This modelling leads us to infer that further work should be done in order to confirm a lower energy for the $c/a < 1$ variant. Another hypothesis is that one cannot assume a constant volume, as volume change is caused by alloying or temperature. In fact, the volume increase within experimental changes of the martensite variants reinforces the minimum for the $c/a < 1$ variant. In addition we have calculated a few new quantities to be measured and encourage new experiments, for instance elastic shear constants in the martensite variants and XAS.

We conclude the explanation of the experimental variants, except for further structural refinements such as shuffling. Although some implications of alloying within a simple model have been discussed, we acknowledge the limitations of the model: we believe that further work on these questions, alloying and/or inclusion of the temperature, may add more insight into this topic. On the other hand, new quantities to be calculated, for instance twin boundaries, constitute at the same time a challenge for further studies.

Acknowledgments

This work has been supported by the Academy of Finland (Centres of Excellence Program 2000–2005) and by the National Technology Agency of Finland (TEKES) and the consortium of Finnish companies (ABB Corporate Research Oy, AdaptaMat Oy, Metso Oyj, Outokumpu Research Oy). AA is supported by the EU TMR programme (contract No ERB4001GT954586). Computer facilities of the Centre for Scientific Computing (CSC) Finland are gratefully acknowledged.

Appendix

As the energy differences involved in figure 2 are tiny, some further comments about the convergence and accuracy are given in the following. As a first comment, the cell volume is kept constant in order to avoid all the computational errors from a change of volume during the tetragonal distortions. Next the dip in the curve of the total energy versus distortions survives during the following tests:

(i) using a different and larger value for $l_{max,ns} = 6$;
(ii) increasing the number of k-points both with the tetrahedron method including the Blöchl linear corrections [31] and with the Fermi smearing method using a small smearing;
(iii) dealing with another correlation scheme within the GGA approach as given in [32] (note that the use of the standard LSD approach [33] makes the dip disappear) and
(iv) using a different way of presenting the lattice, for instance, as a bct structure instead of the fct one, so that different Brillouin zones and different bases are involved.

We remark that the same topology of energy versus distortion is also reproduced by another FLAPW code [34] where all the muffin-tin radii have the same value, 1.19 Å. All these test results seem to justify our confidence in the results presented in figure 2.

References

[1] Brown P J, Bengali A Y, Crangle J, Neuman K-U and Ziebeck K R A 1999 *J. Phys.: Condens. Matter* **11** 4715
[2] Webster P J 1969 *Contemp. Phys.* **10** 559
[3] Webster P J, Ziebeck K R A, Town S L and Peak M S 1984 *Phil. Mag.* **49** 295
[4] Martynov V V 1995 *J. Physique Coll.* IV **5** C8 91
[5] Chernenko V A, Segui C, Cesari E, Pons J and Kokorin V V 1998 *Phys. Rev.* B **57** 2659
[6] Chernenko V A, Cesari E, Kokorin V V and Vitenko I N 1995 *Scr. Metall. Mater.* **33** 1239
[7] Martynov V V and Kokorin V V 1992 *J. Physique* III **2** 739

[8] Worgull J, Petti E and Trivisonno J 1996 *Phys. Rev.* B **54** 15 695
[9] Mañosa L, González-Comas A, Obradó E, Planes A, Chernenko V A, Kokorin V V and Cesari E 1997 *Phys. Rev.* B **55** 11 068
[10] Dong J W, Chen L C, Xie J Q, Müller T A R, Carr D M, Palmstrøm C J, McKernan S, Pan Q and James R D 2000 *J. Appl. Phys.* **88** 7357
[11] Dong J W, Chen L C, Palmstrøm C J, James R D and McKernan S 1999 *Appl. Phys. Lett.* **75** 1443
[12] Mañosa L and Planes A *Adv. Solid State Phys.* at press and references therein
[13] Heczko O, Sozinov A and Ullakko K 2000 *IEEE Trans. Magn.* **36** 3266
Heczko O, Jurek K and Ullakko K 2001 *J. Magn. Magn. Mater.* **226** 996
[14] Murray S J, Marioni M A, Kukla A M, Robinson J, O'Handley R C and Allen S M 2000 *J. Appl. Phys.* **87** 5474
[15] Ayuela A, Enkovaara J, Ullakko K and Nieminen R M 1999 *J. Phys.: Condens. Matter* **11** 2017
[16] James R D and Hane K F 2000 *Acta Mater.* **48** 197
[17] Handley R C O 1998 *J. Appl. Phys.* **83** 3265
[18] Vasilév A N, Bozhko A D, Khovailo V V, Dikshtein I E, Shavrov V G, Buchelnikov V D, Matsumoto M, Suzuki S, Takagi T and Tani J 1999 *Phys. Rev.* B **59** 1113
[19] Godlevsky V V and Rabe K M 2001 *Phys. Rev.* B **63** 134407
[20] Blaha P, Schwarz K and Luitz J 1997 *WIEN97* Vienna University of Technology (an improved and updated Unix version of the copyrighted WIEN code, P Blaha, K Schwarz, P Sorantin and S B Trickey 1990 *Comput. Phys. Commun* **59** 399)
[21] Perdew J P, Burke S and Ernzerhof M 1996 *Phys. Rev. Lett.* **77** 3865
[22] Pons J, Seguí C, Cherneko V A, Cesari E, Ochin P and Portier R 1999 *J. Mater. Sci. Eng.* A **273–275** 315
[23] Sozinov A *et al* 2002 private communication
[24] Enkovaara J, Ayuela A, Nordström L and Nieminen R M 2002 *J. Appl. Phys.* **91** 7798
[25] Fujii S, Ishida S and Asano S 1989 *J. Phys. Soc. Japan* **58** 3657
[26] Enkovaara J 2002 unpublished
[27] Ullakko K *et al* 2001 private communication
[28] Gavriljuk V *et al* 2001 private communication
[29] Plogmann S, Schlathölter T, Braun J, Neumann M, Yarmoshenko Y M, Yablonskikh M V, Shereder E I, Kurmaev E Z, Wrona A and Ślebarski A 1999 *Phys. Rev.* **60** 6428
[30] Ambrosch-Draxl C, Majewski J A, Vogl P and Leising G 1995 *Phys. Rev.* **51** 9668
[31] Blöchl P E, Jepsen O and Andersen O K 1994 *Phys. Rev.* B **49** 16 223
[32] Perdew J P, Vosko J A, Vosko S H, Jackson K A, Pederson M R, Singh D J and Fiolhais C 1992 *Phys. Rev.* B **46** 6671
[33] Perdew J P and Wang Y 1992 *Phys. Rev.* B **45** 13 244 and references therein
[34] Nordström L and Singh D J 1996 *Phys. Rev. Lett.* **76** 4420